On the trail of molecular hydrophilicity and hydrophobicity at aqueous interfaces

Wanlin Chen,[1] Stephanie E. Sanders,[2] Burak Özdamar,[1] Dorian Louaas,[1] Flavio Siro Brigiano,[1,3] Simone Pezzotti,[4,1] Poul B. Petersen,[2] and Marie-Pierre Gaigeot[1]

[1)] *Université Paris-Saclay, Univ Evry, CNRS, LAMBE UMR8587, 91025 Evry-Courcouronnes, France*

[2)] *Department of Chemistry and Biochemistry, Ruhr University Bochum, 44801 Bochum, Germany*

[3)] *Sorbonne Université, Muséum National d'Histoire Naturelle, UMR CNRS 7590, IRD, Institut de Minéralogie, de Physique des Matériaux et de Cosmochimie, IMPMC, F-75005Paris, France*

[4)] *Department of Physical Chemistry II, Ruhr University Bochum, D-44801 Bochum, Germany*

**Corresponding author: Marie-Pierre Gaigeot, mgaigeot@univ-evry.fr*

Dissecting the liquid water organization in contact with hydrophobic and hydrophilic surfaces is essential for understanding the chemical and physical properties of aqueous interfaces. Recently developed descriptors for microscopic hydrophobicity/hydrophilicity based either on molecular dynamics (MD) simulations or on surface-sensitive nonlinear optical techniques, such as sum frequency generation (SFG) spectroscopy, manage to capture and quantify the change in local molecular hydrophobicity at heterogeneous surfaces. However, the connections between the theoretical/structural descriptors and spectroscopic fingerprints have not been established yet. Here, we combine density functional theory-based MD simulations (DFT-MD) and both theoretical and experimental SFG spectroscopy to explore how the interfacial water responds in contact with self-assembled monolayers (SAM) of tunable hydrophilicity. We introduce a microscopic metric to track the transition from hydrophobic to hydrophilic interfaces, which combines a structural descriptor based on the preferential orientation within the water network in the topmost binding interfacial layer (BIL) and spectroscopic fingerprints of H-bonded and dangling OH groups of water pointing towards the surface carried by BIL-resolved SFG spectra. This metric builds a bridge between molecular descriptors of hydrophilicity/hydrophobicity and spectroscopically measured quantities, and provides a recipe to quantitatively or qualitatively interpret experimental SFG signals.

INTRODUCTION

Understanding liquid water organization at solid surfaces is of central importance in many phenomena, encompassing the ability of interfaces to catalyze chemical reactions[1,2], electric double layer formation and adsorption processes[3–5], dielectric response of the interface[6,7], ultrafast energy transfer and vibrational dynamics[8,9], surface acidity and conductivity[10–12]. Following the termination of the bulk hydrogen-bonding (HB) network, the water structure is reorganized at an aqueous interface depending on the balance between water-surface and water-water interactions. Such balance dictates hydrophilicity/hydrophobicity of an interface. It is subtly connected to the nature, morphology, and topology of the hydrated surfaces[13]. These subtle, yet fundamental connections cannot be captured by the conventional macroscopic metric—contact angle—due to the nanoscale structural heterogeneity and dynamics of extended interfaces[3,14,15]. Therefore, there is the need for searching molecular signatures to comprehend microscopic hydrophobicity/hydrophilicity at the nanoscopic scale. Despite enormous progress, this remains a challenge for both theory and experiment[16–18].

In particular, from the experimental side, the surface-sensitive nonlinear optical technique, vibrational sum-frequency generation (SFG) spectroscopy, has been widely utilized to characterize aqueous interfaces at the molecular level[19–26], since the second-order susceptibility $\chi^{(2)}(\omega)$ is zero for centrosymmetric media (like the bulk of liquids and solids). SFG spectroscopy can directly probe dangling OH groups at the interface, which are regarded as a key indicator of molecular hydrophobicity[27–29], as they provide a clear fingerprint in the 3550–3800 cm^{-1} frequency range. Local hydrophobicity at macroscopically hydrophilic surfaces, such as heat-treated silica[15,26] and 0001-α-alumina[30], was hence revealed by the detection of the SFG-active dangling OH groups. However, this signature provides little information on the structure and connectivity of the water HB-network, and does not allow us to quantitatively follow the transition in the interfacial water arrangement from hydrophobic to hydrophilic surfaces. This demands a deeper insight into the specific water network formed at the interface, which can be obtained from molecular dynamics (MD) simulations.

Numerous microscopic descriptors of hydrophobicity have been developed in the last decades through MD simulations, based on density fluctuations[31–33], or orientation probes[34] of interfacial water. Godawat *et al.*[31] demonstrated that large local density fluctuations and higher probabilities of low water density provide clear signatures of hydrophobicity. Based on that, local compressibility has been developed as a powerful theoreti-

cal probe to map microscopic hydrophilicity[33]. Shin *et al.*[34] proposed another approach of probing the interfacial structure through statistical analysis of the orientational configurations of interfacial water molecules. In a recent work, we have shown that the preferential orientation of HBs formed by water in the topmost interfacial layer can be used to determine the degree of local hydrophilicity/hydrophobicity[29]. All these descriptors manage to characterize and quantify the molecular hydrophobicity/hydrophilicity, but the connections between these theoretically determined descriptors and spectroscopic fingerprints are still missing.

Bridging between theoretical and spectroscopic fingerprints of molecular hydrophobicity/hydrophilicity is the aim of the present work. To this end, we investigate a set of aqueous interfaces where water is in contact with self-assembled monolayers (SAM) of well-controlled and tunable hydrophilicity. These interfaces have attracted considerable attention as a model platform to study hydrophobicity/hydrophilicity and have been extensively characterized in a number of theoretical[13,35,36] and SFG experimental[37–40] works. We have carried out DFT-MD simulations for three different silane-based SAM/water interfaces (with SAMs anchored on a silica substrate as illustrated in Fig. 1): pure octadecyltrichlorosilane (OTS, $CH_3(–CH_2)_{17}–SiCl_3$) monolayer (intrinsically hydrophobic), pure polyethylene glycol (PEG, $CH_3(OCH_2CH_2)_7CH_2SiCl_3$) monolayer (intrinsically hydrophilic), and mixed OTS-PEG monolayer (1:1 mixing ratio), corresponding to the experimental samples prepared by Sanders *et al.*[40]. The water theoretical SFG spectra of the three interfaces are calculated from the simulations and compared with the experimental measurements[40]. The deconvolution of the water SFG spectra aids to elucidate the macroscopic and molecular response of the interfacial water with increasing hydrophilicity of the SAM surface. On the macroscopic scale, we evaluate the ability of the interface to screen the surface field arising from the charged silica+SAM surface, as obtained by introducing a mixed theoretical and experimental approach to extract the potential drop in the liquid from SFG spectra. On the molecular scale, we adopt quantitative descriptors of hydrophilicity/hydrophobicity based either on the preferential orientation within the water HB-network in the topmost interfacial layer, hereafter named H/V ratio, or on the integration of the SFG intensity in the spectral regions containing the stretching motions of either H-bonded (3000–3550 cm^{-1}) or dangling (3550–3800 cm^{-1}) water OH groups. The synergic evaluation of these molecular and macroscopic descriptors allows us to establish a connection between the structural and spectroscopic fingerprints of molecular hydrophobicity and to map the transition of the water HB network from the most hydrophobic to the most hydrophilic interface.

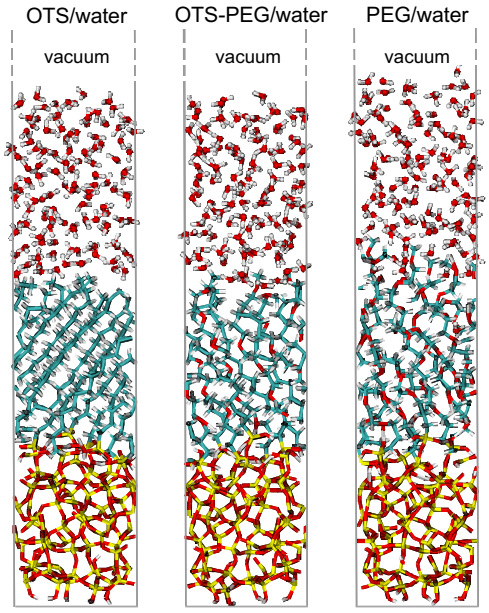

FIG. 1. Snapshots of the three SAM/water interfaces from the DFT-MD simulations. From bottom to top: amorphous silica, SAMs, water, and vacuum (Si: yellow, C: cyan, O: red, H: white). Box dimensions: 13.386×13.286×85 Å^3.

RESULTS AND DISCUSSIONS

Surface potential determination from SFG spectra

Fig. 2A displays the DFT-MD calculated $\mathrm{Im}\chi^{(2)}_{ssp}(\omega)$ spectra of water within the OH stretching region from 3000 to 3800 cm^{-1} for the three SAM/water interfaces presented in Fig. 1. The theoretical spectra are in good agreement with the corresponding experimental spectra measured by Sanders *et al.*[40] and depicted in Fig. 2B. For all systems, the SFG spectra show two bands centered at 3200 and 3400 cm^{-1}, with the intensities decreasing in the order: water/OTS > water/PEG > water/mixed OTS and PEG. An extra peak at around 3660 cm^{-1} corresponding to the signal of the free OH groups is seen at the OTS/water interface.

The consistency between the experimental and the DFT-MD calculated SFG spectra validates our simulations, but the interpretation of the spectra in terms of the water structures interacting with SAMs is still not straightforward due to the following reason. With the silica substrate (below the SAM monolayers, see Fig. 1) negatively charged at the experimental environment (pH∼5.6), the centrosymmetry of bulk-like water located further than the first few angstroms from the interface is broken by the surface electric field. That leads to a non-negligible surface-charge induced contribution to the total SFG signal, which veils the spectrum arising from the specific interfacial structure (the binding interfacial layer, denoted as BIL)[41,42]. Therefore, the understanding of SFG spectra requires the separation of the spectroscopic contributions into a $\chi^{(2)}_{BIL}(\omega)$ contribution arising from

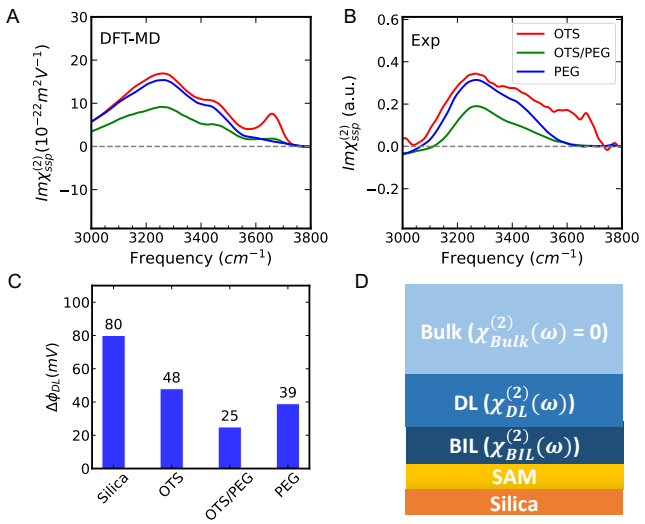

FIG. 2. SFG spectra of the three SAM aqueous interfaces (OTS/water, OTS-PEG/water, PEG/water) in the SSP polarization: (A) DFT-MD calculated spectra of $\mathrm{Im}\chi^{(2)}_{BIL}(\omega)$ under PZC (pH 2∼4) conditions plus fitted $\mathrm{Im}\chi^{(2)}_{DL}(\omega)$ contribution (B) Experimental spectra measured by Sanders *et al.*[40] at pH ∼ 5.6. (C) Potential differences across the liquid region (mV) for the three different systems at pH ∼ 5.6 together with the reference value for the silica/water interface at pH ∼ 6[5]. (D) Scheme of the deconvolution of water SFG spectra into signals arising from water in the binding interfacial layer (BIL) and in the diffuse layer (DL) respectively.

the BIL, the layer directly in contact with the SAMs, and into the contribution from the DL (diffuse layer), $\chi^{(2)}_{DL}(\omega)$, *i.e.* the subsequent layer with bulk-like water reoriented by the surface charges (see Fig. 2D)[41,42]:

$$\chi^{(2)}(\omega) = \chi^{(2)}_{BIL}(\omega) + \chi^{(2)}_{DL}(\omega) \tag{1}$$

The methodology of the deconvolution of $\chi^{(2)}_{BIL}(\omega)$ and $\chi^{(2)}_{DL}(\omega)$ contributions based on the identification of BIL and DL according to three structural descriptors (density, HB network, and orientation) is presented in ref[42].

The $\mathrm{Im}\chi^{(2)}_{BIL}(\omega)$ water spectra are directly calculated from the DFT-MD simulations of the three SAM/water interfaces in the PZC (Point of Zero Charge) conditions (pH 2∼4) where only water in the BIL is noncentrosymmetric and thus SFG active in the OH stretching region (3000–3800 cm^{-1}). The calculation of the $\mathrm{Im}\chi^{(2)}_{DL}(\omega)$ contribution at the experimental pH∼5.6 condition requires much thicker water slabs, than the length-scale affordable in the DFT-MD simulations. However, the $\mathrm{Im}\chi^{(2)}_{DL}(\omega)$ calculation can be achieved after combining with the experimental spectra. At the experimental pH∼5.6, the silica surface is only ∼1% dehydroxylated[43]. Since the $\chi^{(2)}_{BIL}(\omega)$ of a charged interface with a low surface charge density σ (less than a few percent of a monolayer) is barely modified compared to the neutral interfaces, as proved by Tian *et al.*[37,41], we assume $\mathrm{Im}\chi^{(2)}_{BIL}(\omega)$ to be invariant from pH 2–4 to 5.6. The experimentally measured $\mathrm{Im}\chi^{(2)}(\omega)$ is thus equivalent to the sum of the theoretical $\mathrm{Im}\chi^{(2)}_{BIL}(\omega)$ of the fully hydroxylated surface and the charge-induced $\mathrm{Im}\chi^{(2)}_{DL}(\omega)$ contribution.

The field-induced reorientation of water dominates the SFG signal of the DL, which thus contains the interfacial electrostatic information. $\chi^{(2)}_{DL}(\omega)$ is equal to the third-order susceptibility of liquid water, $\chi^{(3)}_{Bulk}(\omega)$, multiplied by the surface potential difference across the DL region, $\Delta\phi_{DL}$, as expressed by:

$$\chi^{(2)}_{DL}(\omega) = \chi^{(3)}_{Bulk}(\omega) \cdot \Delta\phi_{DL} \tag{2}$$

Interference contributions are omitted from the above equation since they are negligible at the experimental condition (ionic strength $> 10^{-2}$ M). The $\chi^{(3)}_{Bulk}(\omega)$ is a constant spectrum for any aqueous interface with two bands centered at 3200 and 3400 cm^{-1}, as demonstrated both experimentally[41] and theoretically[42,44]. $\Delta\phi_{DL}$ solely determines the sign and magnitude of $\chi^{(2)}_{DL}(\omega)$. Although $\Delta\phi_{DL}$ is is actually the surface potential across the DL region, it is usually regarded as the surface potential in the literature. The difference between the surface potential and $\Delta\phi_{DL}$ is determined by the screening within the BIL region. $\Delta\phi_{DL}$ can be extracted from the measured SFG intensities by using Eq. 2, once $\chi^{(3)}_{Bulk}(\omega)$ and $\chi^{(2)}_{DL}(\omega)$ are known.

To achieve this, we combine the total experimental SFG intensity and the theoretical $\chi^{(2)}_{BIL}(\omega)$ spectrum. We start by making a simple consideration: the intensity of the SFG signal in the H-bonded region (3000–3550 cm^{-1}) is the result of the combination of $\chi^{(2)}_{BIL}(\omega)$ and $\chi^{(2)}_{DL}(\omega)$ contributions, while the signal at 3660 cm^{-1} arising from the free OH groups solely contains the $\chi^{(2)}_{BIL}(\omega)$ part. With the calculated $\chi^{(2)}_{BIL}(\omega)$ intensity being fixed, the relative intensity of the free OH signal and the H-bonded band is hence a function of $\chi^{(2)}_{DL}(\omega)$ intensity, which in turns depends on $\Delta\phi_{DL}$ according to Eq. 2. Based on this, the experimental relative intensity of the two bands can be used as an objective function (OF) to determine $\Delta\phi_{DL}$ from a fitting procedure, as expressed by:

$$\begin{aligned} OF &= \frac{\chi^{(2)}_{exp}(\omega_{freeOH})}{\chi^{(2)}_{exp}(\omega_{Hbonded})} \\ &= \frac{\chi^{(2)}_{BIL}(\omega_{freeOH})}{\chi^{(2)}_{BIL}(\omega_{Hbonded}) + \Delta\phi_{DL} \cdot \chi^{(3)}_{bulk}(\omega_{Hbonded})} \end{aligned} \tag{3}$$

where $\chi^{(2)}_{exp}(\omega)$ is the experimental SFG spectrum, $\chi^{(2)}_{BIL}(\omega)$ and $\chi^{(3)}_{bulk}(\omega)$ are theoretical spectra calcutated from the DFT-MD simulations, with $\omega_{freeOH} = 3660$ cm^{-1}, and $\omega_{Hbonded} = 3250$ cm^{-1}. This methodology makes it possible to extract the $\Delta\phi_{DL}$ of the interface directly from the experimentally measured SFG spectrum, without knowing its absolute intensity. The $\Delta\phi_{DL}$ values

providing the best fit for all three interfaces are plotted in Fig. 2C.

Compared to the reference $\Delta\phi_{DL}$ value (80 mV) at the silica/water interface at pH∼6 from ref[5], the obtained $\Delta\phi_{DL}$ values for the three SAM/water interfaces are well reduced. This indicates that the presence of monolayers between water and the silica substrate has a screening effect on the surface charge, with $\Delta\phi_{DL}$ decreasing in the order OTS (48 mV) > PEG (39 mV) > mixed OTS-PEG (25 mV). Intrinsically, PEG polymer chains screen better than OTS chains because of their larger dipole moments due to the presence of oxygen atoms. However, this still can not explain the strongest screening effect of the mixed OTS-PEG monolayer. With the assumption that the different degrees of screening effect might also be related to the organization of the SAM chains, we refer to the results of Sanders *et al.*[40], where a qualitative investigation of the spatial order of the three monolayers is introduced by evaluating the relative intensity of methylene to methyl SFG bands. Their results show that the OTS monolayer is uniform and well ordered, whereas the PEG chains are significantly more disordered than the OTS due to the variable chain length of the commercial silane (6-9 PEG units), which allows the longer chains to lean over shorter chains. The mixed OTS-PEG monolayer is the most disordered monolayer, as expected, due to the implicit PEG disorder and the defects and disorders generated by the mixture of OTS and PEG. The decrease in the SAM chain order (OTS > PEG > OTS/PEG) is qualitatively correlated with the increase in the screening effect: the more disordered the monolayer, the stronger the surface charge is reduced.

Another possible explanation can be thought by considering that the screening comes from not only the monolayer but also the organization of BIL-water. BIL-water is horizontally ordered (2DN) above a hydrophobic surface[29,45] and vertically ordered at a hydrophilic one[15,46,47]. At the mixed interfaces with the coexistence of microscopic hydrophobic and hydrophilic patches, it is disordered with neither a stable 2DN nor a stable vertically ordered structure. The BIL-water organization at the three SAM-water interfaces is characterized in the next section.

Interpretation of $\chi^{(2)}_{BIL}(\omega)$

The specific interfacial structures of water adapting to various surfaces are revealed by the SFG signal of the BIL. Fig. 3B shows the $\mathrm{Im}\chi^{(2)}_{BIL}(\omega)$ spectra of the three different interfaces calculated from the DFT-MD simulations over ∼ 400 ps for each system. The BIL spectrum of the OTS/water interface resembles that of the hydrophobic prototype—the air/water interface[45]—with a positive peak at 3660 cm^{-1}, corresponding to the dangling OH groups pointing towards the monolayer as shown by green circles in Fig. 3A on top, and a broad negative band centered at around 3350 cm^{-1}. It is noted

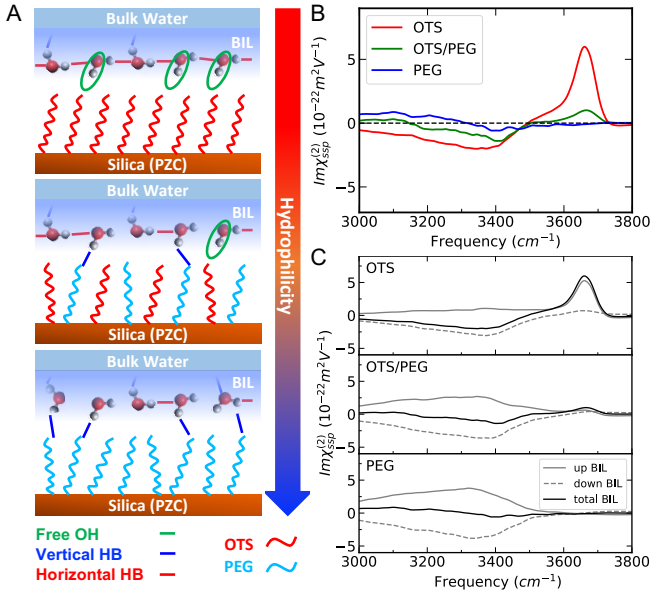

FIG. 3. Characterizations of BIL water structures in contact with the three different monolayers: (A) Scheme of different types of OH groups of BIL water. (B) DFT-MD calculated $\mathrm{Im}\chi^{(2)}_{BIL}(\omega)$ signals. (C) Deconvoloved water-up and water-down BIL spectra.

that the frequency of the free OH peak is lower than that of the air/water interface, which we ascribe to the van der Waals interactions between the dangling OH and the OTS monolayer as suggested by Tian *et al.*[37]. A similar shift is also observed in the SFG spectra of water in contact with graphene and boron-nitride (BN)[29]. The mixed OTS-PEG/water SFG spectrum also presents a free OH peak and a broad negative band in the H-bonded region, but with strongly reduced intensities. The PEG spectrum unexpectedly shows an almost zero signal over the whole O-H stretching region. The disappearance of the free OH peak is reasonable, but the minuscule signal in the H-bonded region is astonishing.

As mentioned above, one strength of the DFT-MD SFG compared to the experimental one is that we can further deconvolve the BIL-water spectrum by calculating the spectral contributions arising from each BIL-water population identified from the simulations based on structural properties. Knowing that the normal in SFG is the vector perpendicular and pointing to the solid surface, we have deconvolved the BIL spectra into signals arising from water molecules with their dipole moment pointing towards the SAMs (along the normal, thus denoted as 'up') and the ones pointing towards the subsequent bulk water (opposite to the normal, thus 'down'). The two deconvolved spectra are denoted as water-up and water-down, respectively, and displayed in Fig. 3C.

Strikingly, the water-up and water-down spectra of the PEG/water interface are both broad bands centered at ∼ 3300 cm^{-1}, with the same intensity and opposite sign, and the compensation of the two leads to an approximate

zero signal in total. The same frequency of the water-up and water-down spectra indicates that the strength of H-bonds formed between the oxygen atoms of PEG and water in the BIL is the same as that of water-water H-bonds between BIL and bulk. For mixed OTS-PEG/water, we observe a similar compensation of water-up and water-down broad bands in the H-bonded region, which explains the very low intensity of the negative band seen in the total BIL spectrum compared to the OTS/water spectrum.

Spectroscopic and structural descriptors of microscopic hydrophilicity/hydrophobicity

The free OH peak revealed by SFG spectroscopy is a well-recognized microscopic hydrophobic fingerprint[27–29]. It is thus quantified here by calculating the $\mathrm{Im}\chi^{(2)}_{BIL}(\omega)$ integral in the 3550–3800 cm^{-1} region for each SAM interface (Fig. 4A, red bars). The integrals decrease with the increase of the number of PEG chains in the monolayer composition. Interestingly, the integral of the mixed OTS-PEG/water free OH signal is $\sim$ five times smaller than that of the pure OTS/water interface, despite OTS and PEG are mixed in a 1:1 ratio (which is expected to result in a decrease by a factor of ~ 2). The reason for this over-suppression of the free-OH SFG signal at the mixed SAM/water interface is topological: most of the water molecules in contact with OTS units point their OH groups toward nearby PEG chains, as they can interact with O-atoms of PEGs, thus leaving only very few dangling OH groups. This result indicates that the hydrophilic sites dictate the water-surface interactions, and they can suppress molecular hydrophobicity (as measured by free-OH groups) around the OTS chains for uniform mixing of OTS and PEG. In other words, the spatial distribution of the hydrophobic/hydrophilic sites has a large influence on global hydrophobicity, as it is well documented in previous theoretical works.[33,48? –51]. As a result of dangling-OH suppression for the uniform mixing adopted in our simulation, the tiny free OH peak in the BIL-SFG spectrum of the mixed PEG-OTS/water system is hardly distinguishable from the PEG/water interface, both with approximately zero free OH signal. It is thus difficult to microscopically quantify the degree of hydrophilicity of the SAM/water interfaces solely by the free OH signature in SFG.

We thus introduce a different descriptor based on the molecular details of the interfacial water structure that are accessible from DFT-MD simulations. Above a hydrophobic surface, water molecules in the BIL form preferential horizontal water-water H-bonds, which leads to a two-dimensional HB network (2DN) structure[29,45], whereas vertical ordered structures based on surface-water H-bonds are favored above a hydrophilic surface[15,46,47]. Therefore, apart from the free OH peak in the SFG spectrum, the hydrophilicity can be evaluated by quantifying the number of horizontal water-water H-bonds and the number of vertical surface-water H-bonds formed in the BIL.

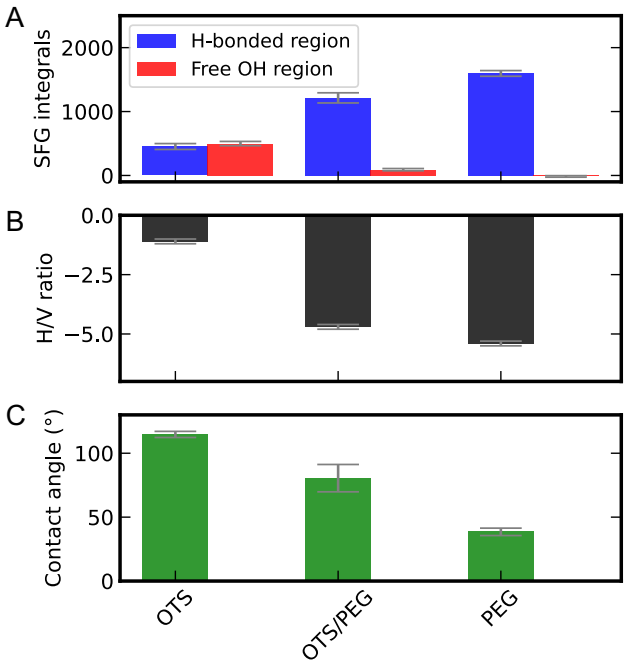

FIG. 4. Hydrophobicity/hydrophilicity descriptors investigated in this work. Two microscopic descriptors determined from SFG signals and DFT-MD simultaions: (A) SFG intensity integrals of the deconvolved water-up spectra in the spectral regions of the free-OH (3550–3800 cm^{-1}) and H-bonded (3000–3550 cm^{-1}) OH stretching motions, and (B) structural descriptor based on the preferential orientation within the water network in the binding interfacial layer (BIL)—H/V ratios. One macroscopic descriptor: (C) contact angles measured by Sanders *et al.*[40]

To that end, the first approach is to quantify the H-bonds by integrating the SFG signals in the H-bonded region from 3000 cm^{-1} to 3550 cm^{-1}. Since the horizontal H-bonded OH groups are SFG inactive, the integral of the H-bonded signal in the SFG spectrum solely contains the vertical components of the H-bonded OH groups. However, as shown above, the signals arising from OH groups H-bonded to the O atoms of PEGs are washed out in the total BIL spectra, because of the compensation between water-up and water-down contributions due to the same strength of PEG-water and water-water H-bonds. We hence choose to calculate the integral of the deconvolved water-up signal, in order to account for the water-surface H-bonds. The larger this integral is, the more vertical H-bonds are formed between BIL-water and the SAMs, hence the more hydrophilic the surface is. The results are shown in Fig. 4A in blue bars. As expected, the integrals of these H-bond signals (blue) are anticorrelated with the ones of the free OH signal (red). Furthermore, the difference in hydrophilicity between the mixed OTS-

PEG/water and the PEG/water can now be captured by this indicator.

Another approach is to directly calculate the densities of horizontal HBs ($N_{HBs}(H)/nm^2$) and vertical HBs ($N_{HBs}(V)/nm^2$) from the DFT-MD simulations and define the horizontal/vertical ratio (H/V ratio) as a descriptor to quantify the hydrophobicity/hydrophilicity of the surface. The horizontal H-bonds are defined as H-bonds formed between BIL-waters and parallel to the surface $\pm$ 30° (red lines in Fig. 3A). The vertical H-bonds are defined as the water-surface H-bonds[45] (blue lines in Fig. 3A). Instead of directly calculating the ratio, we add the value one to the denominator in Eq. 4 to prevent it from being zero for the pure OTS/water system, where there are no water-surface H-bonds. To ease the comparison, the H/V ratios discussed in the following are referenced to the value calculated for the air/water interface—the hydrophobic prototype. The H/V ratio is thus:

$$H/V\ ratio = \frac{N_{HBs}(H)/nm^2}{1 + N_{HBs}(V)/nm^2} - H/V\ ratio\,(Air/Water) \quad (4)$$

Therefore, an interface with a H/V ratio close to zero is an interface as hydrophobic as the air/water interface, and the more negative the H/V ratio is, the more hydrophilic the interface is.

The H/V ratios calculated for the three SAM/water interfaces, statistically averaged over $\sim$ 400 ps of trajectory for each system, are plotted in Fig. 4B. The values are correlated with the integral values of the H-bonded SFG signal (Fig. 4A, blue bars) and anticorrelated with the integral values of the free OH signal (Fig. 4A, red bars). The H/V ratio values range from -1.1 for the pure OTS/water interface to -5.4 for the pure PEG/water interface. A value of -4.7 is obtained for the mixed OTS-PEG/water interface in between the two extreme values. The H/V ratio of -1.1 signifies that the OTS/water interface is less hydrophobic than the reference air/water interface, which is consistent with the red shift of the free OH peak of the OTS/water SFG spectrum with respect to the one of the air/water interface (due to the van der Waals interactions between the free OH groups and the OTS at the interface[37]). The H/V value for the mixed OTS-PEG/water interface (-4.7) is closer to that of the PEG/water interface (-5.4) compared to the OTS/water interface. This confirms the dominating effect of the hydrophilic sites on the global hydrophobicity of the interface implied by the large decrease of the free OH peak intensity compared to the OTS/water interface as discussed above.

The values of the macroscopic hydrophilicity descriptor—contact angle—measured by Sanders *et al.*[40] (Fig. 4C) show in general the same trend as the two DFT-MD and SFG spectral-based microscopic metrics. The contact angles range from 114.7° (pure OTS, hydrophobic) to 38.5° (pure PEG, hydrophilic), but the reported value of a mixed OTS-PEG/water sample (80.5°) is closer to that of the pure OTS than to the pure PEG in contrary to our descriptors. The more hydrophilic behavior of our simulated mixed OTS-PEG/water interface reiterates the relevance of topological patterns over the surface: the homogeneous distribution of OTS and PEG chains imposed in our DFT-MD simulation is a case that minimizes surface hydrophobicity (as discussed above), while the experimental mixed SAM surface seems to display a larger heterogeneity in terms of PEG/OTS distribution, giving rise to larger hydrophobic (i.e. OTS rich) patches and larger local hydrophobicity.

CONCLUSIONS

Local hydrophobicity plays an essential role in the chemical and physical properties of heterogeneous aqueous interfaces. It is usually experimentally probed by SFG spectroscopy following the signature provided by the water dangling OH groups pointing towards a hydrophobic surface. Although powerful and straightforward to use, this fingerprint alone fails to capture the collective structural organization of the water HB network as a function of surface hydrophilicity, which ultimately dictates interfacial properties. In this work, we combined DFT-MD simulations and SFG spectroscopy to go deeper into this molecular complexity. We found that the orientation of the water HB network in the topmost binding interfacial layer (BIL) well describes the collective molecular organization of the liquid water when it adapts to surfaces. In particular, we have shown that such orientation describes well the changes in the HB network when going from a horizontally (H) ordered HB network formed between BIL water molecules in the most hydrophobic environments to a vertical (V) ordering dominated by HBs between a hydrophilic surface and BIL water molecules. These structural changes have a direct signature in the SFG spectra since $\chi^{(2)}(\omega)$ is sensitive to molecular orientation, while horizontally oriented water molecules have negligible activity. Therefore, the SFG intensity of the BIL in the OH stretching region directly measures the degree of H/V ordering, and thus local hydrophobicity/hydrophilicity.

However, quantitatively evaluating these changes from the total SFG spectra of charged interfaces, like the SAM/water interfaces presented here, can be challenging since it requires deconvolution of the spectrum of the BIL from that of the subsequent DL, where water is reoriented by the static field generated by a charged surface. Moreover, contributions from vertically oriented water molecules in the BIL can cancel out if water molecules pointing toward the surface and toward the bulk form HBs with similar strength, as was the case for the PEG/water interface. For these reasons, quantitative estimations of surface hydrophilicity from SFG spectra require theoretical SFG spectroscopy, as it naturally provides the deconvolution of all of these contributions. By combining the experimental and deconvolved theoretical

SFG spectra, we showed here that the structural H/V ratio descriptor, the BIL SFG intensity, and macroscopic contact angle measurements were all correlated for the investigated SAM/water interfaces, giving a picture of local surface hydrophobicity/hydrophilicity that extends from the molecular to the macroscopic range.

In cases where theoretical SFG spectroscopy is not available, our work still provides a recipe to experimentally assess molecular hydrophobicity and hydrophilicity qualitatively. That requires the $\chi^{(2)}_{BIL}(\omega)$ to be separated from the total SFG spectrum, which can be achieved by adopting experimental state-of-the-art deconvolution schemes[30,41,52,53]. For a given surface, local hydrophobicity and hydrophilicity can be efficiently tuned by playing with parameters such as the pre-treatment of the surface, the applied potential (for electrochemical interfaces)[6,30,54], the pH[5] and the ionic strength[52,53]. In these cases, changes in the total SFG intensity in the OH stretching region of the BIL spectrum can be directly used to qualitatively identify and interpret changes in surface hydrophilicity. To give a practical example, the addition of salt to the amorphous silica/water interface was shown by DFT-MD simulations to promote the in-plane organization of the BIL water network[5], therefore increasing the hydrophobicity of the interface. This was indeed experimentally captured by the decrease in the integrations of the BIL SFG spectra at pH $\sim$ 2 (PZC) with increasing ionic strength[5]. In the future, our metric that connects the H/V ratio (structural descriptor) to the integrals of $\chi^{(2)}_{BIL}(\omega)$ in the H-bonded region can be broadly applied to organic and oxide interfaces. It can be used to detect local hydrophobicity/hydrophilicity from SFG experiments, either qualitatively (experiments alone) or quantitatively by combining with theoretical SFG spectroscopy.

COMPUTATIONAL METHODOLOGY

Born-Oppenheimer DFT-MD simulations are carried out with the CP2K package[55,56], adopting the BLYP[57,58] electronic representation with Grimme D2 corrections[59,60] for dispersion, GTH pseudopotentials, and a combined Plane-Wave (400 Ry density cutoff) and DZVP-SR MOLOPT basis set. The Newton's equations of motions are integrated through the Velocity Verlet algorithm for the nuclei with a 0.4 fs time step. The simulation boxes of $13.386 \times 13.286 \times 85.0$ $\mathring{A}^3$ are each composed of eight SAM chains (corresponding to the experimental samples in Ref.[40]) anchored to an amorphous silica surface with a hydroxylation degree of 4.5 SiOH/nm^2, solvated by 120 water molecules. The amorphous silica model is taken from Ugliengo *et al.*[61], it can accommodate up to 8 SiOH groups at the surface at PZC conditions, see refs[15,47]. The 8 SiOH groups are replaced by 8 polymeric chains. Three different systems are built with 8 OTS chains (pure OTS/water), alternately mixing of 4 OTS and 4 PEG chains (mixed OTS-PEG/water), and 8 PEG chains (pure PEG/water), respectively. Each box is periodically repeated in the x and y directions and separated by a vacuum layer of 25 $\mathring{A}$ from the replica in the vertical z-direction. For each system, four individual trajectories are accumulated with initial configurations extracted from different geometry optimization steps. The DFT-MD simulations are composed of 10 ps of equilibration for each trajectory before the production run of 100 ps, both in the NVE ensemble (with velocity rescaling and a target temperature of 300 K in the equilibration part only).

The SFG signal, coming from the imaginary component of the total resonant electric dipole nonlinear susceptibility $\chi^{(2)}(\omega)$ is calculated following the time-dependent approach of Morita *et al.*[38,62] For the water contribution to $\chi^{(2)}(\omega)$, individual molecular dipole moments and polarizability tensors are calculated with the model from ref[63], supposing that only the OH stretching motions contribute to the spectrum in the high frequency region ($>$ 3000 cm^{-1}). All details of derivation for the expression of SFG can be found in ref[42,47] with the parameterization of APT and Raman tensors of water found in ref[63]. Each SFG spectrum is calculated from an average over $\sim$ 400 ps DFT-MD.

For all structural analyses, we have adopted the H-bond definition proposed by White and co-workers[64], with $O(-H)\cdots O \leq 3.2$ Å and the $O-H\cdots O$ angle between 140° and 220°.

ACKNOWLEDGMENTS

This work was performed under PRACE (Partnership for Advanced Computing in Europe) under No. 2018194688. We acknowledge PRACE for awarding access to the Fenix infrastructures at GENCI-TGCC-France, which are partially funded from the European Union's Horizon 2020 research and innovation program through the ICEI project under the grant agreement No. 800858. We also acknowledge HPC resources from GENCI-France Grant 072484 (CINES/IDRIS/TGCC).

AUTHOR DECLARATIONS

Conflict of interest

The authors have no conflicts to disclose.

DATA AVAILABILITY STATEMENT

The data that support the findings of this study are available from the corresponding authors upon reasonable request.

[1] J. Zhu, L. Hu, P. Zhao, L. Y. S. Lee, and K.-Y. Wong, *Chem. Rev.*, 2019, **120**(2), 851–918.

[2]F. S. Brigiano, M. Gierada, F. Tielens, and F. Pietrucci, *ACS Catal.*, 2022, **12**, 2821–2830.
[3]A. Serva, M. Salanne, M. Havenith, and S. Pezzotti, *Proc. Natl. Acad. Sci.*, 2021, **118**(15).
[4]S. R. Alfarano, S. Pezzotti, C. J. Stein, Z. Lin, F. Sebastiani, S. Funke, C. Hoberg, I. Kolling, C. Y. Ma, K. Mauelshagen, T. Ockelmann, G. Schwaab, L. Fu, J.-B. Brubach, P. Roy, M. Head-Gordon, K. Tschulik, M.-P. Gaigeot, and M. Havenith, *Proc. Natl. Acad. Sci.*, 2021, **118**(47).
[5]A. Tuladhar, S. Dewan, S. Pezzotti, F. S. Brigiano, F. Creazzo, M.-P. Gaigeot, and E. Borguet, *J. Am. Chem. Soc.*, 2020, **142**(15), 6991–7000.
[6]A. Montenegro, C. Dutta, M. Mammetkuliev, H. Shi, B. Hou, D. Bhattacharyya, B. Zhao, S. B. Cronin, and A. V. Benderskii, *Nature*, 2021, **594**(7861), 62–65.
[7]C. Qi, Z. Zhu, C. Wang, and Y. Zheng, *J. Phys. Chem. Lett.*, 2021, **12**(2), 931–937.
[8]M. J. DelloStritto, S. M. Piontek, M. L. Klein, and E. Borguet, *J. Phys. Chem. Lett.*, 2019, **10**(9), 2031–2036.
[9]S. M. Piontek and E. Borguet, *J. Phys. Chem. C*, 2022, **126**(5), 2307–2324.
[10]F. Giberti and A. A. Hassanali, *J. Chem. Phys.*, 2017, **146**(24), 244703.
[11]S. Pezzotti and M.-P. Gaigeot, *Atmosphere*, 2018, **9**(10), 396.
[12]B. Grosjean, M.-L. Bocquet, and R. Vuilleumier, *Nat. Commun.*, 2019, **10**(1), 1–8.
[13]J. Monroe, M. Barry, A. DeStefano, P. Aydogan Gokturk, S. Jiao, D. Robinson-Brown, T. Webber, E. J. Crumlin, S. Han, and M. S. Shell, *Annu. Rev. Chem. Biomol.*, 2020, **11**, 523–557.
[14]D. T. Limmer, A. P. Willard, P. Madden, and D. Chandler, *Proc. Natl. Acad. Sci.*, 2013, **110**(11), 4200–4205.
[15]J. D. Cyran, M. A. Donovan, D. Vollmer, F. S. Brigiano, S. Pezzotti, D. R. Galimberti, M.-P. Gaigeot, M. Bonn, and E. H. Backus, *Proc. Natl. Acad. Sci.*, 2019, **116**(5), 1520–1525.
[16]G. Galli, *Proc. Natl. Acad. Sci.*, 2007, **104**(8), 2557–2558.
[17]J.-L. Li, R. Car, C. Tang, and N. S. Wingreen, *Proc. Natl. Acad. Sci.*, 2007, **104**(8), 2626–2630.
[18]K. Rana, S. A. Boyd, B. J. Teppen, H. Li, C. Liu, and C. T. Johnston, *Phys. Chem. Chem. Phys.*, 2009, **11**(16), 2976–2985.
[19]Y. Shen, *Fundamentals of sum-frequency spectroscopy*, Cambridge University Press, 2016.
[20]Q. Du, R. Superfine, E. Freysz, and Y. Shen, *Phys. Rev. Lett.*, 1993, **70**(15), 2313.
[21]A. Eftekhari-Bafrooei and E. Borguet, *J. Am. Chem. Soc.*, 2010, **132**(11), 3756–3761.
[22]Z. Zhang, L. Piatkowski, H. J. Bakker, and M. Bonn, *Nat. Chem.*, 2011, **3**(11), 888–893.
[23]C.-S. Hsieh, M. Okuno, J. Hunger, E. H. Backus, Y. Nagata, and M. Bonn, *Angew. Chem. Int. Ed.*, 2014, **53**(31), 8146–8149.
[24]C. Tian and Y. Shen, *Surf. Sci. Rep.*, 2014, **69**(2-3), 105–131.
[25]A. M. Jubb, W. Hua, and H. C. Allen, *Annu. Rev. Phys. Chem.*, 2012, **63**, 107–130.
[26]L. Dalstein, E. Potapova, and E. Tyrode, *Phys. Chem. Chem. Phys.*, 2017, **19**(16), 10343–10349.
[27]F. Tang, T. Ohto, S. Sun, J. R. Rouxel, S. Imoto, E. H. Backus, S. Mukamel, M. Bonn, and Y. Nagata, *Chem. Rev.*, 2020, **120**(8), 3633–3667.
[28]Q. Du, E. Freysz, and Y. R. Shen, *Science*, 1994, **264**(5160), 826–828.
[29]S. Pezzotti, A. Serva, F. Sebastiani, F. S. Brigiano, D. R. Galimberti, L. Potier, S. Alfarano, G. Schwaab, M. Havenith, and M.-P. Gaigeot, *J. Phys. Chem. Lett.*, 2021, **12**(15), 3827–3836.
[30]H. Wang, Q. Xu, Z. Liu, Y. Tang, G. Wei, Y. R. Shen, and W.-T. Liu, *J. Phys. Chem. Lett.*, 2019, **10**(19), 5943–5948.
[31]R. Godawat, S. N. Jamadagni, and S. Garde, *Proc. Natl. Acad. Sci.*, 2009, **106**(36), 15119–15124.
[32]A. J. Patel, P. Varilly, and D. Chandler, *J. Phys. Chem. B*, 2010, **114**(4), 1632–1637.
[33]H. Acharya, S. Vembanur, S. N. Jamadagni, and S. Garde, *Faraday Discuss.*, 2010, **146**, 353–365.
[34]S. Shin and A. P. Willard, *J. Comput. Chem.*, 2018, **14**(2), 461–465.
[35]J. I. Monroe and M. S. Shell, *Proc. Natl. Acad. Sci.*, 2018, **115**(32), 8093–8098.
[36]B. C. Dallin and R. C. Van Lehn, *J. Phys. Chem. Lett.*, 2019, **10**(14), 3991–3997.
[37]C. Tian and Y. Shen, *Proc. Natl. Acad. Sci.*, 2009, **106**(36), 15148–15153.
[38]A. Morita and T. Ishiyama, *Phys. Chem. Chem. Phys.*, 2008, **10**(38), 5801–5816.
[39]S. Ye, S. Nihonyanagi, and K. Uosaki, *Phys. Chem. Chem. Phys.*, 2001, **3**(16), 3463–3469.
[40]S. E. Sanders and P. B. Petersen, *J. Chem. Phys.*, 2019, **150**(20), 204708.
[41]Y.-C. Wen, S. Zha, X. Liu, S. Yang, P. Guo, G. Shi, H. Fang, Y. R. Shen, and C. Tian, *Phys. Rev. Lett.*, 2016, **116**(1), 016101.
[42]S. Pezzotti, D. R. Galimberti, Y. R. Shen, and M.-P. Gaigeot, *Phys. Chem. Chem. Phys.*, 2018, **20**(7), 5190–5199.
[43]P. M. Dove, *Am. J. Sci.*, 1994, **294**(6), 665–712.
[44]T. Joutsuka, T. Hirano, M. Sprik, and A. Morita, *Phys. Chem. Chem. Phys.*, 2018, **20**(5), 3040–3053.
[45]S. Pezzotti, D. R. Galimberti, and M.-P. Gaigeot, *J. Phys. Chem. Lett.*, 2017, **8**(13), 3133–3141.
[46]M. Sulpizi, M.-P. Gaigeot, and M. Sprik, *J. Comput. Chem.*, 2012, **8**(3), 1037–1047.
[47]S. Pezzotti, D. R. Galimberti, and M.-P. Gaigeot, *Phys. Chem. Chem. Phys.*, 2019, **21**(40), 22188–22202.
[48]N. B. Rego, E. Xi, and A. J. Patel, *Proc. Natl. Acad. Sci.*, 2021, **118**(6).
[49]S. N. Jamadagni, R. Godawat, and S. Garde, *Annu. Rev. Chem. Biomol.*, 2011, **2**, 147–171.
[50]E. Xi, V. Venkateshwaran, L. Li, N. Rego, A. J. Patel, and S. Garde, *Proc. Natl. Acad. Sci.*, 2017, **114**(51), 13345–13350.
[51]N. Giovambattista, P. G. Debenedetti, and P. J. Rossky, *J. Phys. Chem. C*, 2007, **111**(3), 1323–1332.
[52]S.-h. Urashima, A. Myalitsin, S. Nihonyanagi, and T. Tahara, *J. Phys. Chem. Lett.*, 2018, **9**(14), 4109–4114.
[53]E. H. Backus, J. Schaefer, and M. Bonn, *Angew. Chem. Int. Ed.*, 2021, **60**(19), 10482–10501.
[54]Y. Zhang, H. B. de Aguiar, J. T. Hynes, and D. Laage, *J. Phys. Chem. Lett.*, 2020, **11**(3), 624–631.
[55]J. Hutter, M. Iannuzzi, F. Schiffmann, and J. VandeVondele, *Wiley Interdiscip. Rev. Comput. Mol. Sci.*, 2014, **4**(1), 15–25.
[56]J. VandeVondele, M. Krack, F. Mohamed, M. Parrinello, T. Chassaing, and J. Hutter, *Comput. Phys. Commun.*, 2005, **167**(2), 103–128.
[57]A. D. Becke, *Phys. Rev. A*, 1988, **38**(6), 3098.
[58]C. Lee, W. Yang, and R. G. Parr, *Phys. Rev. B*, 1988, **37**(2), 785.
[59]S. Grimme, *J. Comput. Chem.*, 2004, **25**(12), 1463–1473.
[60]S. Grimme, *J. Comput. Chem.*, 2006, **27**(15), 1787–1799.
[61]P. Ugliengo, M. Sodupe, F. Musso, I. Bush, R. Orlando, and R. Dovesi, *Adv. Mater.*, 2008, **20**(23), 4579–4583.
[62]A. Morita and J. T. Hynes, *J. Phys. Chem. B*, 2002, **106**(3), 673–685.
[63]R. Khatib, E. H. Backus, M. Bonn, M.-J. Perez-Haro, M.-P. Gaigeot, and M. Sulpizi, *Sci. Rep.*, 2016, **6**(1), 1–10.
[64]J. A. White, E. Schwegler, G. Galli, and F. Gygi, *J. Chem. Phys.*, 2000, **113**(11), 4668–4673.